Mix-and-extrude using 3D printed nozzles for time-resolved membrane protein crystallography

Mohammad Vakili*‡, Huijong Han*‡, Christina Schmidt, Agnieszka Wrona, Marco Kloos, Iñaki de Diego, Katerina Dörner, Joana Valerio, Ekaterina Round, Kristina Lorenzen and Joachim Schulz*

European XFEL GmbH, Holzkoppel 4, 22869 Schenefeld, Germany

*Correspondence emails: mohammad.vakili@xfel.eu; huijong.han@xfel.eu; joachim.schulz@xfel.eu

‡MV and HH contributed equally to this work.

Synopsis 3D printed mixing-HVE devices address time-resolved membrane protein crystallography challenges via compact dual-flow LCP injection.

Abstract Time-resolved crystallography enabled the visualization of protein molecular motion during reaction. Currently, light is the most prevalent reaction initiator, but the number of light-activated proteins is extremely limited. Instead, more biological reactions are triggered by interaction with ligands. To examine the molecular action of these mixing-initiated reactions by X-ray diffraction, a sample delivery method that allows for diffusive mixing of crystals with ligands in a short amount of time corresponding to the reaction time to be studied is needed. This paper describes the mix-and-extrude nozzle for delivering membrane proteins crystallized in lipid cubic phase and ligands, along with its preliminary characterization and outlook for future developments.

Keywords: Time-resolved serial crystallography; mix-and-extrude; 3D printed nozzle

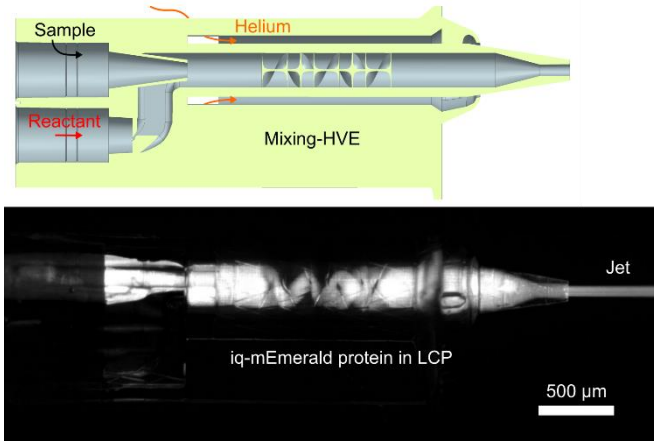

1. Introduction

Membrane proteins comprise about 23% of all proteins (Uhlén *et al.*, 2015). They play an essential role in biological function and are the target of numerous medications on the market (Overington *et al.*, 2006). Due to sample preparation challenges, the number of membrane protein structures that have been determined is rather low despite their biological significance. For rational drug design, the structures of target protein of apo and ligand-bound forms are essential to understand mode of action. In addition, the emerging time-resolved crystallography would provide a better perspective of the structure in motion by ligand binding.

By employing lipid cubic phase (LCP) as a medium, membrane protein crystallization was facilitated (Landau & Rosenbusch, 1996; Li & Caffrey, 2020). The LCP features a unique lipid bilayer and aqueous channel structure that is continuous, folded, and highly curved. During crystallization, the cubic phase is locally converted to the lamellar phase by equilibrating with precipitant solutions, and the protein is concentrated in the lamellar phase to form a nucleus and ultimately a crystal (Cherezov & Caffrey, 2007; Caffrey, 2008). Multiple characterization studies demonstrated the mobility of chemicals and proteins in LCP via lipidic or aqueous phases (Cherezov *et al.*, 2006; Li *et al.*, 2017; Li & Caffrey, 2011; Clogston & Caffrey, 2005; Eriksson & Lindblom, 1993; Boland *et al.*, 2018), indicating that LCP can be used as a medium for biochemical/biophysical characterization in addition to crystallization of membrane proteins.

Sample delivery for time-resolved serial crystallography with light-sensitive protein crystals is not different from the ones for serial crystallography for static structure determination; the only difference in the set-up is the additional light source, often a laser, to initiate the reaction. Time-resolved study of ligand binding, on the other hand, needs an additional liquid channel for the ligand. For crystals grown in aqueous solution, mix-and-inject schemes using liquid jets (Pandey *et al.*, 2021; Hejazian *et al.*, 2020; Calvey *et al.*, 2016) or adding/injecting ligand on top of crystals for fixed target, drop-on-demand and tape-drive have been developed as sample delivery for time-resolved serial crystallography (Mehrabi *et al.*, 2019; Butryn *et al.*, 2021; Beyerlein *et al.*, 2017).

The high-viscosity extruder (HVE), created by Weierstall *et al.*, is one of the most widely used sample delivery methods for membrane protein crystals in serial crystallography (Weierstall *et al.*, 2014). Within this HVE, a hydraulic plunger is used to amplify the pressure provided by an HPLC pump 14 times. This can provide the pressure up to 10,000 psi to drive the sample from the sample reservoir into the capillary and the nozzle. Compared with glass syringes, which can withstand pressures of up to 1,000 psi, this type of injection is more reliable for delivering viscous samples.

Three-dimensional (3D) printing using two-photon polymerization (2PP) enables a rapid, reproducible and high-throughput nozzle fabrication, in addition to design flexibility (Knoška *et al.*, 2020). Recently, we presented our portfolio of 3D printed sample delivery devices, including HVE injection tips that provide controllable viscous sample streams (Vakili *et al.*, 2022). Here, we introduce the 3D

printed mix-and-extrude nozzle, which was designed for the simultaneous use of two HVE setups. The device provides a second capillary port for introducing a ligand dispersed in viscous medium. With this, the mixing of two samples immediately before X-ray probing can be achieved. The 3D printed mixing-HVE nozzle is anticipated to enable time-resolved crystallography of membrane protein crystals for the investigation of ligand-binding reactions.

2. Materials and Methods

2.1. Design choices

The mixer ("J_7") provides a dual-inlet section accepting two capillaries and allowing the convergence of two fluid channels via overlapping concentric cones (Fig. 1A). At the start of the mixing channel, the main/side channel diameter ratio is 100:231.7 µm. Due to the centered sample inlet and the 3D hydrodynamic flow-focusing, a wall contact of the sample is prevented. The total length of the mixing channel is 2570 µm. From this length, the initial 2070 µm have a 231.7 µm channel width, followed by a 300 µm long tapering section (truncated cone which reduces the ID down to 75 µm), leading to a 200 µm long final section with 75 µm in diameter. For the geometry at the tip, the ID-OD-D (liquid channel diameter-gas orifice-distance between orifices) are chosen to be 75-345-600 [µm], therefore, 75 µm wide streams are provided for the X-ray beam.

Inside the first section of the 231.7 µm wide mixing channel, a modified mixing structure based on the "JKMH#10" Kenics mixer from Knoška and Heymann (Knoška *et al.*, 2020), is incorporated. With this, a series of six helical elements are introduced into the mixing channel for repeated flow splitting/stretching. The first blade is positioned 500 µm after the mixing initiation point (overlap of the liquid apertures).

From previous studies, it is known that flow velocities as low as v = 0.3 mm/s are sufficient for stable vicious extrusion while avoiding the exposure of the same crystal with multiple X-ray pulses at 10 Hz repetition rate (Vakili *et al.*, 2022).

With the 2570 µm long mixing channel and a combined liquid flow rate of Q_{total} = 2.1 µL/min (*i.e.* 2 µL/min for the reactant and 0.1 µL/min for the sample), a retention time of 3.0 s before extrusion can be achieved within the 3D printed part. This corresponds to a stream velocity of v_{flow} = 7.9 mm/s for the 75 µm wide sample stream. Longer retention times require lower flow rates. For instance, a retention time of 18.1 s can be obtained with Q_{total} = 0.36 µL/min (exposed sample has a velocity v_{flow} = 1.3 mm/s). Another design variation ("J_8") contains a shorter mixing channel (1685 µm). With the aforementioned flow rates, the shorter mixer allows retention times between 1.6 s and 9.8 s.

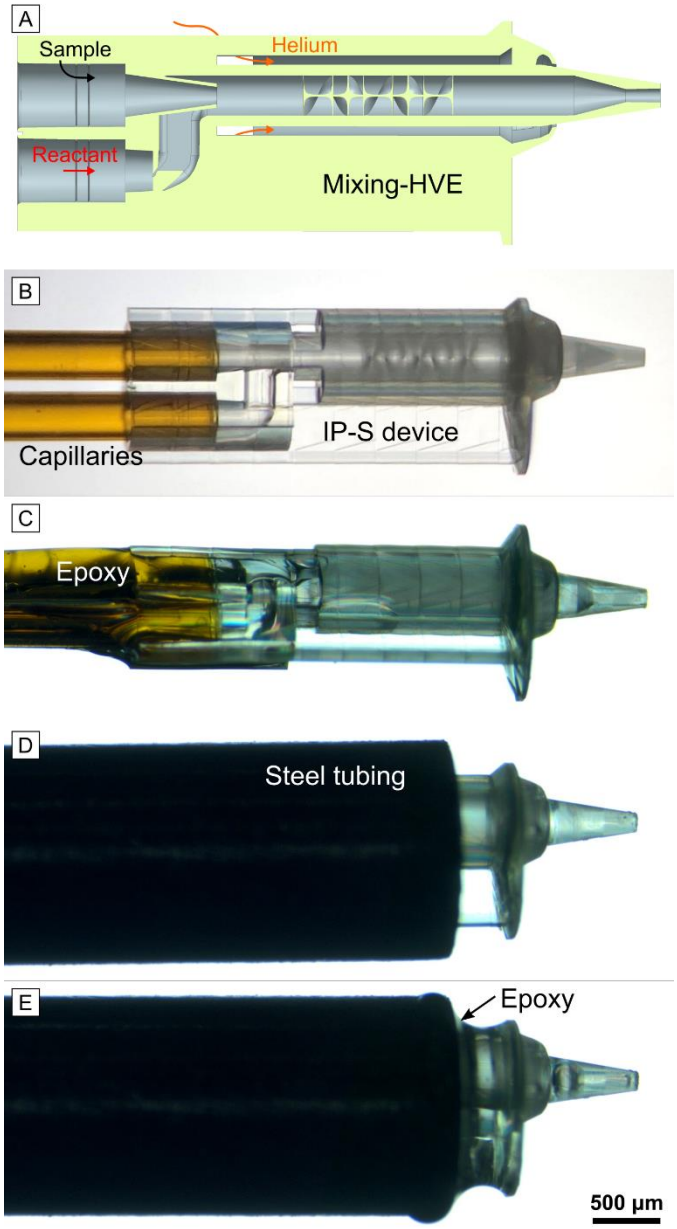

Figure 1 (A) Cross-sectional schematic depiction of the 2PP-3D printed mix-and-extrude device. (B-E) Microscopy images showing the assembly of the mixing-HVE tip with two fluid-feeding fused silica capillaries. (B) Two capillaries, each with 250 µm ID, are inserted into the 3D printed mixing-HVE's access ports and (C) glued with epoxy glue. (D) The capillaries (un-glued end) are fiddled through a 0.046'' ID steel tubing, which is pulled over the mixing section of the device. (E) A small amount of slightly viscous epoxy glue (cured for 2 min) is added onto the gap with a clean capillary or metal wire to secure IP-S to the steel and provide gas tightness.

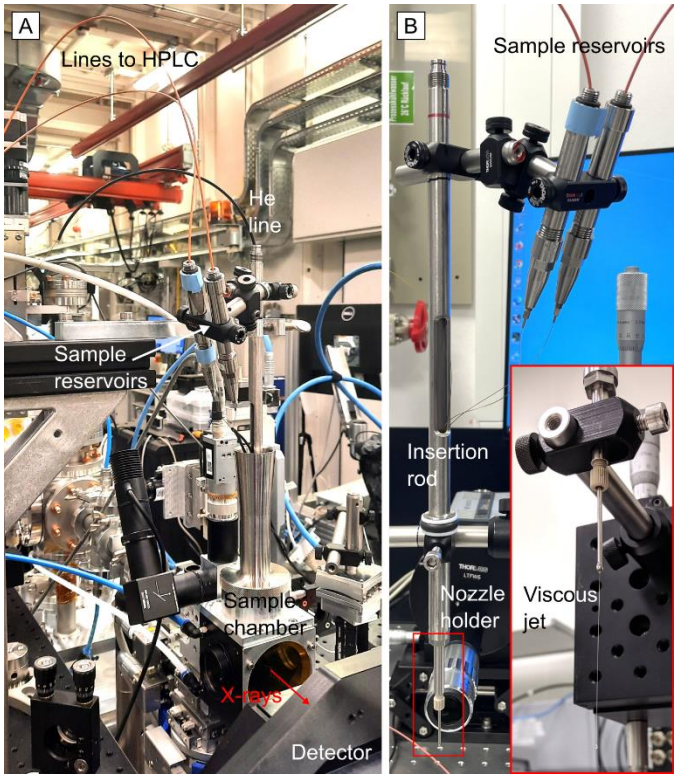

Figure 2 Beamline injection setup surrounding the mixing-HVE device inside the helium-purged sample chamber at the SPB/SFX instrument (A) and in the test station during in-air operation (B).

2.2. Beamtime injection setup

The SPB/SFX instrument of the European XFEL comprises two interaction regions, a high-vacuum upstream sample environment (Interaction Region Upstream, IRU) and an in-helium downstream interaction region (Interaction Region Downstream, IRD) with respect to the X-ray beam. The instrument setup at IRD provides high flexibility on sample deliveries, including the HVE injection setup. The injection rod funnel attached helium atmosphere sample chamber is located between vacuum out-coupling acoustic delay line (ADL) and detector (JUNGFRAU 4M), and the inserted nozzle rod is positioned using XYZ motors of the goniometer support tower (Round *et al*., in preparation).

The assembled nozzle, connected to capillaries and the U-145 steel tubing, was connected to the nozzle holder using a F333N fitting (IDEX). A slit on the insertion rod (Fig. S1B) was created 10 cm above the o-ring to shorten the sample capillary length. After screwing the nozzle holder onto the metal rod and inserting the rod into the IRD sample chamber, the capillaries were carefully taken through the slit and linked to the sample reservoirs of the HVEs using 0.015-0.0625" ID PEEK (polyether ether ketone) tubing and custom #10-32 UNF steel fitting with 1/16" through-hole (similar to F-354, IDEX). Using ThorLab ½” mounting rods, the two HVE systems were mounted onto the insertion rod to bridge the short distance to the nozzle (Fig. 2A). The final capillary length was 30 cm, with an interior volume of 14.7 µL.

2.3. Sample preparation

The preparation of iq-mEmerald protein and crystal is described in supplementary information, and following procedures were included to prepare the samples suitable for HVE injection. The LCP was prepared with a 7:3 ratio of monoolein to water using two gas tight glass syringes and a coupler. To embed iq-mEmerald crystals and $CuCl_2$ in LCP, 10% (v/v) crystal pellet and 20 mM $CuCl_2$ solution were mixed with prepared LCP separately. For mixing investigation inside the nozzle, iq-mEmerald protein embedded in LCP was used instead of protein crystals to observe continuous fluorescence signal; 65:35 ratio of monoolein and 10 mg/mL of iq-mEmerald protein in 50 mM Tris (pH 8.0) or 10 mM $CuCl_2$ was mixed and resulted in 130 µM protein and 3.5 mM $CuCl_2$ in LCP, respectively (Fig. 3). The prepared samples were loaded into HVE sample reservoirs and prepared for injection.

The samples were extruded using two HPLC pumps (Shimadzu, LC-20AD XR) connected to the two HVE injector systems (Weierstall *et al.*, 2014). The pumps were first run rapidly to fill the capillary with samples (up to 2.14 µL/min). When the extruded sample volume was determined to be around 13 µL, shortly before the samples reached the nozzle, the flow rates were reduced to the desired values.

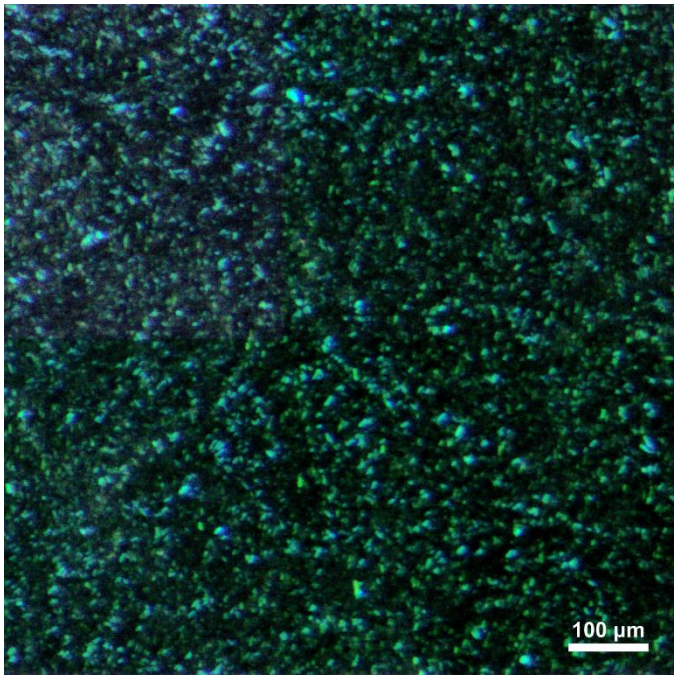

Figure 3 Stereomicroscopy image of iq-mEmerald crystals (*ca.* 5×15 µm) embedded in LCP, used for the mix-and-extrude nozzle characterization.

3. Results and Discussion

3.1. Nozzle characterization

We chose iq-mEmerald fluorescence quenched by copper ions as the test system for mix-and-extrude nozzle characterization because it is easy to visualize. Moreover, the reaction time is so fast that it can be ignored in the mixing time scale of our nozzle, and the diffusion time of copper ion is expected to be fast compared with other ligands. The mixing ratio of crystal and copper ions was fixed to 1:3 so that the concentration of copper does not affect the quenching time and fluorescence intensity. The retention time for the characterization was triggered between 2.3 and 7.6 seconds (Fig. S4). The same injection test was performed under a fluorescence microscope for quenching observation in high resolution. The fluorescence in the nozzle tip area was recorded, and the quenching of the crystals by copper ions was observed (Movie S1). Independent of the retention time, we could observe fluorescence quenching of mixed species within the jet, meaning that the diffusion of copper ions in LCP and the quenching reaction in iq-mEmerald crystals happened faster than 2.3 seconds. The diffusion and the reaction of the test system was very fast thus the fluorescence signal disappeared even before the sample was extruded from the nozzle. To measure how fast this diffusion and reaction happens within the mixing device, we reduced the intrinsic fluorescence of the IP-S photoresist by curing the device in a UV (λ = 385 nm) chamber (XYZprinting, 3UD10XEU01K) followed by hard-baking at 80 °C for 3 hours As shown in Fig. 4, a mixing time of approximately 1.8 s can be estimated based on the travelled distance of 1.02 mm (from 'Inlet' to the downstream 'Mixer' position).

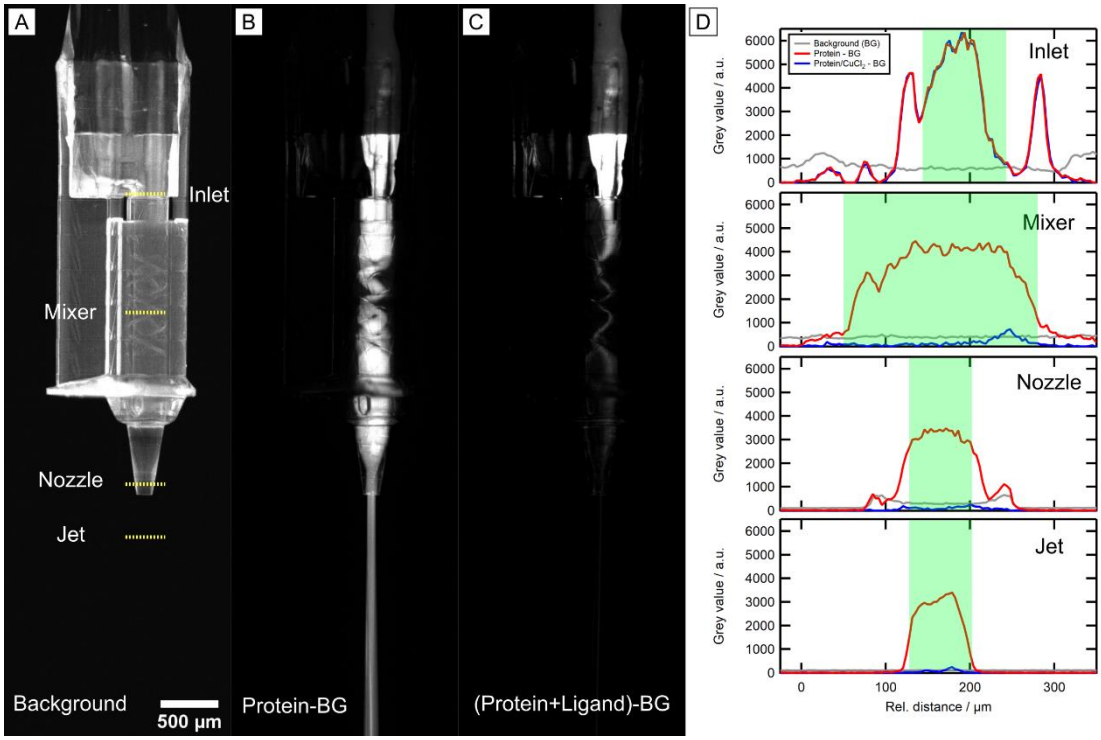

Figure 4 Observation of fluorescence quenching inside the 3D printed mixing-HVE device. (A) Fluorescence microscopy image of the empty IP-S mixing-HVE device which serves as the background image. (B) Background-corrected image of the sample, *i.e.* iq-mEmerald protein (130

µM) flowing at 0.36 µL/min in the nozzle. (C) Background-corrected image showing the mixing of iq-mEmerald (130 µM) and $CuCl_2$ (3.5 mM) entering with a 1:3 flow rate ratio (0.36 and 1.07 µL/min, respectively). The corresponding total retention time amounts to *ca.* 4.4 s. (D) Pixel intensity profiles from the 16-bit fluorescence images (relative grey values extracted via ImageJ 1.53k) for four downstream positions: inside the 100 µm wide sample orifice (Inlet) , inside the 231.7 µm wide mixing channel within the Kenics section, 1 mm downstream from the inlet (Mixer), within the final, 75 µm wide section of the device material before extrusion (nozzle) and in-air, 300 µm away from the nozzle tip (jet) . The positions are denoted with the yellow-dotted lines in (A). The green boxes in (D) indicate the geometric restrictions of the device/jet. The fluorescence signal at the 'Mixer' position (mixing time: 1.8 s) has decreased to *ca.* 10% of the initial 130 µM concentration from 'Inlet' and there is no significant fluorescence signal inside the 'Jet' indicating full quenching upon mixing.

3.2. Diffusion in LCP

One of the biggest challenges in time-resolved serial crystallography, which determines distinct intermediate structures throughout the reaction, remains the rapid mixing of microcrystal with ligands (Brändén & Neutze, 2021; Schmidt, 2013). Even in investigations using aqueous solutions, the diffusion time of ligand to the crystal's center varies based on crystal size and packing, i.e. crystals in smaller sizes or having a higher water content per unit cell are unquestionably better candidates for time-resolved crystallography, as the ligand diffusion time would be decreased for such crystals. For membrane protein crystals in LCP, diffusion is even more challenging. LCP has a similar packing structure to crystals, with the exception of a wider water channel than protein crystals. In addition, the thickness of the LCP stream inserted from a capillary is 231.7 µm, which increases the diffusion time by 3.1 seconds for oxygen and 13.2 seconds for glucose by calculation if the ligands are assumed to diffuse directly into the center of the LCP stream (Atkins & Paula, 2006). To reduce such diffusion time caused by the width of the stream, a Kenics architecture was employed in our mixing channel to support the mixing of crystal and ligand in LCP. With the series of helical elements for repeated flow splitting/stretching, we exponentially increase the diffusive interface with each additional element. Mixing time point uniformity/dispersion becomes more dependent on spatial location along the mixer and highly insensitive to flow rate fluctuations. This feature is in contrast to flow-focusing designs that tune diffusion distances through flow rate differentials. Even with these efforts to obtain discrete intermediates by reducing diffusion time, it is still likely to observe a mixture of multiple intermediates by mixing with this nozzle. With current advancements in data analysis (*e.g.* Xtrapol8, (De Zitter *et al.*, 2022)), it is projected that mixed diffraction data of multiple states can be separated.

Due to the complexity of the LCP structure and membrane protein, it is difficult to predict the diffusion and reaction time of ligand binding in LCP; for instance, if the ligand is diffused in an aqueous channel and the binding site of membrane protein is located in an aqueous channel, the

diffusion time would be comparable to that of in aqueous solution. Alternatively, if the binding occurs in the lipid, it is likely too time-consuming to be studied using this type of nozzle. Therefore, we assume that this nozzle is suited for the examination of reactions taking place on the cell/membrane surface, where most current drugs targeting membrane protein act on (Yin & Flynn, 2016). However, due to this overall unpredictability of reaction in LCP, it is highly recommended to characterize the reactions in LCP prior to X-ray diffraction using different biochemical and biophysical techniques in order to confirm that the reaction takes place on a timescale compatible to the operation of these nozzles.

3.3. Future development

The current setup, which utilizes external fluid-feeding capillaries, is susceptible to rupture. Moreover, sample-conserving inner diameters below 250 µm are prone to generate high pressures during injection. It is also worth noting that the used capillary length of 30 cm generated a void volume of 14.7 µL. Especially when considering the difficulties of membrane protein sample preparation and the available sample reservoir capacities of 40 and 120 µL, this sample loss of 14.7 µL is not negligible. To reduce the length of the capillaries, a more compact mixing-HVE composed of two hydraulic systems within a single, protective injector rod is desired. In addition, large injection infrastructure is difficult to be installed at the beamline, which is already occupied with significant instrumentation (detector, laser setup, electronics, optics, and etc.). Thus, a small injection footprint should be maintained.

In the HVE used in our experiment, the sample reservoir is screwed into the hydraulic system and the capillary is connected to the sample reservoir in the same manner, however, this way of connection does not work when two capillaries glued in a nozzle on the other end must be in fixed places. In the design of the other type of HVE described in the recent publication by Shimazu *et al.* (Shimazu *et al.*, 2019), the capillary connection to the sample reservoir does not require direct screwing. Thus, we assume that adaptation of this design would make it possible to create a compact mixing-HVE. Currently the planning and designing of such a device are in progress.

As described above, diffusion time of diluted species in LCP media is difficult to predict. To cover a broader range of diffusion and reaction time, modification on the nozzle is under consideration. For shorter retention time, the length of the mixer can be reduced. To access longer retention, a modular assembly approach can be pursued in which the printed mixer and nozzle are connected by a capillary extension of custom length. In addition, once the compact mixing HVE is ready and shorter capillaries can be used, the ID of capillaries and mixer/nozzle can be reduced because pressure build-up due to long capillaries is not a concern anymore. Then, even higher sample flow rates can be applied to the system: with faster sample movement in the mixer, the retention time can be reduced further.

4. Conclusion

We fabricated and characterized a mix-and-extrude nozzle for time-resolved membrane protein serial crystallography. Fluorescence quenching by mixing iq-mEmerald crystals with copper ions was observed on a short timescale, indicating that the diffusion in LCP occurred in a negligible time compared to the retention time of the mixer. With current designs of the nozzle, a retention time between *ca.* 1 and 20 seconds can be triggered, and nozzles aiming for shorter and longer retention time can be prepared with minor design modification. The first user experiment using this nozzle at IRD@SPB/SFX at the European XFEL has been conducted and the manuscript describing the result is currently in preparation. We anticipate that this mix-and-extrude nozzle will be widely used for mixing experiments with membrane protein crystals at synchrotrons and FELs, hence, efforts to create a mixing-HVE as a single compact system are ongoing.

Acknowledgements The authors would like to thank all members of the EuXFEL SEC group for their excellent teamwork and scientific interaction, as well as the instrument scientists at the SPB/SFX instrument for their support and helpful discussions. We also thank Thomas Dietze and Marco Schrage (EuXFEL) for CNC machining. We further express our gratitude to Richard Neutze (University of Gothenburg), Juraj Knoška (Center for Free-Electron Laser Science, Hamburg) and Michael Heymann (University of Stuttgart) for fruitful discussions.

References

Atkins, P. & Paula, J. De (2006). Atkins' Physical chemistry 8th edition.

Beyerlein, K. R., Dierksmeyer, D., Mariani, V., Kuhn, M., Sarrou, I., Ottaviano, A., Awel, S., Knoska, J., Fuglerud, S., Jönsson, O., Stern, S., Wiedorn, M. O., Yefanov, O., Adriano, L., Bean, R., Burkhardt, A., Fischer, P., Heymann, M., Horke, D. A., Jungnickel, K. E. J., Kovaleva, E., Lorbeer, O., Metz, M., Meyer, J., Morgan, A., Pande, K., Panneerselvam, S., Seuring, C., Tolstikova, A., Lieske, J., Aplin, S., Roessle, M., White, T. A., Chapman, H. N., Meents, A. & Oberthuer, D. (2017). *IUCrJ*. **4**, 769–777.

Boland, C., Olatunji, S., Bailey, J., Howe, N., Weichert, D., Fetics, S. K., Yu, X., Merino-Gracia, J., Delsaut, C. & Caffrey, M. (2018). *Anal. Chem.* **90**, 12152–12160.

Brändén, G. & Neutze, R. (2021). *Science (80-.).* **373**, eaba0954.

Butryn, A., Simon, P. S., Aller, P., Hinchliffe, P., Massad, R. N., Leen, G., Tooke, C. L., Bogacz, I., Kim, I. S., Bhowmick, A., Brewster, A. S., Devenish, N. E., Brem, J., Kamps, J. J. A. G., Lang, P. A., Rabe, P., Axford, D., Beale, J. H., Davy, B., Ebrahim, A., Orlans, J., Storm, S. L. S., Zhou, T., Owada, S., Tanaka, R., Tono, K., Evans, G., Owen, R. L., Houle, F. A., Sauter, N. K.,

Schofield, C. J., Spencer, J., Yachandra, V. K., Yano, J., Kern, J. F. & Orville, A. M. (2021). *Nat. Commun.* **12**, 4461.

Caffrey, M. (2008). *Crystal Growth and Design*, Vol. *8*, pp. 4244–4254.

Calvey, G. D., Katz, A. M., Schaffer, C. B. & Pollack, L. (2016). *Struct. Dyn.* **3**, 054301.

Cherezov, V. & Caffrey, M. (2007). *Faraday Discuss.* **136**, 195–212.

Cherezov, V., Clogston, J., Papiz, M. Z. & Caffrey, M. (2006). *J. Mol. Biol.* **357**, 1605–1618.

Clogston, J. & Caffrey, M. (2005). *J. Control. Release*. **107**, 97–111.

Eriksson, P. O. & Lindblom, G. (1993). *Biophys. J.* **64**, 129–136.

Hejazian, M., Darmanin, C., Balaur, E. & Abbey, B. (2020). *RSC Adv.* **10**,.

Knoška, J., Adriano, L., Awel, S., Beyerlein, K. R., Yefanov, O., Oberthuer, D., Peña Murillo, G. E., Roth, N., Sarrou, I., Villanueva-Perez, P., Wiedorn, M. O., Wilde, F., Bajt, S., Chapman, H. N. & Heymann, M. (2020). *Nat. Commun.* **11**, 657.

Landau, E. M. & Rosenbusch, J. P. (1996). *Proc. Natl. Acad. Sci. U. S. A.* **93**, 14532–14535.

Li, D. & Caffrey, M. (2011). *Proc. Natl. Acad. Sci. U. S. A.* **108**, 8639–8644.

Li, D. & Caffrey, M. (2020). *J. Mol. Biol.* **432**, 5104–5123.

Li, Z., Tang, Y., Wu, Y., Zhao, S., Bao, J., Luo, Y. & Li, D. (2017). *Nat. Commun.* **8**, 1691.

Mehrabi, P., Schulz, E. C., Agthe, M., Horrell, S., Bourenkov, G., von Stetten, D., Leimkohl, J. P., Schikora, H., Schneider, T. R., Pearson, A. R., Tellkamp, F. & Miller, R. J. D. (2019). *Nat. Methods*. **16**, 979–982.

Overington, J. P., Al-Lazikani, B. & Hopkins, A. L. (2006). *Nat. Rev. Drug Discov.* **5**, 993–996.

Pandey, S., Calvey, G., Katz, A. M., Malla, T. N., Koua, F. H. M., Martin-Garcia, J. M., Poudyal, I., Yang, J. H., Vakili, M., Yefanov, O., Zielinski, K. A., Bajt, S., Awel, S., Doerner, K., Frank, M., Gelisio, L., Jernigan, R., Kirkwood, H., Kloos, M., Koliyadu, J., Mariani, V., Miller, M. D., Mills, G., Nelson, G., Olmos, J. L., Sadri, A., Sato, T., Tolstikova, A., Xu, W., Ourmazd, A., Spence, J. C. H., Schwander, P., Barty, A., Chapman, H. N., Fromme, P., Mancuso, A. P., Phillips, G. N., Bean, R., Pollack, L. & Schmidt, M. (2021). *IUCrJ*. **8**, 878–895.

Samarkina, O. N., Popova, A. G., Gvozdik, E. Y., Chkalina, A. V., Zvyagin, I. V., Rylova, Y. V., Rudenko, N. V., Lusta, K. A., Kelmanson, I. V., Gorokhovatsky, A. Y. & Vinokurov, L. M. (2009). *Protein Expr. Purif.* **65**, 108–113.

Schmidt, M. (2013). *Adv. Condens. Matter Phys.* **2013**, 167276.

Shimazu, Y., Tono, K., Tanaka, T., Yamanaka, Y., Nakane, T., Mori, C., Kimura, K. T., Fujiwara, T., Sugahara, M., Tanaka, R., Doak, R. B., Shimamura, T., Iwata, S., Nango, E. & Yabashi, M. (2019). *J. Appl. Crystallogr.* **52**, 1280–1288.

Uhlén, M., Fagerberg, L., Hallström, B. M., Lindskog, C., Oksvold, P., Mardinoglu, A., Sivertsson, Å., Kampf, C., Sjöstedt, E., Asplund, A., Olsson, I. M., Edlund, K., Lundberg, E., Navani, S., Szigyarto, C. A. K., Odeberg, J., Djureinovic, D., Takanen, J. O., Hober, S., Alm, T., Edqvist, P. H., Berling, H., Tegel, H., Mulder, J., Rockberg, J., Nilsson, P., Schwenk, J. M., Hamsten, M.,

Von Feilitzen, K., Forsberg, M., Persson, L., Johansson, F., Zwahlen, M., Von Heijne, G., Nielsen, J. & Pontén, F. (2015). *Science (80-.).* **347**, 1260419.

Vakili, M., Bielecki, J., Knoška, J., Otte, F., Han, H., Kloos, M., Schubert, R., Delmas, E., Mills, G., De Wijn, R., Letrun, R., Dold, S., Bean, R., Round, A., Kim, Y., Lima, F. A., Dörner, K., Valerio, J., Heymann, M., Mancuso, A. P. & Schulz, J. (2022). *J. Synchrotron Radiat.* **29**, 331–346.

Weierstall, U. (2014). *Philos. Trans. R. Soc. B Biol. Sci.* **369**, 20130337.

Weierstall, U., James, D., Wang, C., White, T. A., Wang, D., Liu, W., Spence, J. C. H., Bruce Doak, R., Nelson, G., Fromme, P., Fromme, R., Grotjohann, I., Kupitz, C., Zatsepin, N. A., Liu, H., Basu, S., Wacker, D., Won Han, G., Katritch, V., Boutet, S., Messerschmidt, M., Williams, G. J., Koglin, J. E., Marvin Seibert, M., Klinker, M., Gati, C., Shoeman, R. L., Barty, A., Chapman, H. N., Kirian, R. A., Beyerlein, K. R., Stevens, R. C., Li, D., Shah, S. T. A., Howe, N., Caffrey, M. & Cherezov, V. (2014). *Nat. Commun.* **5**, 3309.

Yin, H. & Flynn, A. D. (2016). *Annu. Rev. Biomed. Eng.* **18**,.

Yu, X., Strub, M. P., Barnard, T. J., Noinaj, N., Piszczek, G., Buchanan, S. K. & Taraska, J. W. (2014). *PLoS One*. **9**, e95808.

De Zitter, E., Coquelle, N., Oeser, P., Barends, T. R. M. & Colletier, J. P. (2022). *Commun. Biol.* **5**, 640.